AIP | Applied Physics Letters

Anti-reflection resonance in distributed Bragg reflectors-based ultrathin highly absorbing dielectric and its application in solar cells

Xu-Lin Zhang, Jun-Feng Song, Xian-Bin Li, Jing Feng, and Hong-Bo Sun

Citation: Applied Physics Letters **102**, 103901 (2013); doi: 10.1063/1.4795286
View online: http://dx.doi.org/10.1063/1.4795286
View Table of Contents: http://scitation.aip.org/content/aip/journal/apl/102/10?ver=pdfcov
Published by the AIP Publishing

Anti-reflection resonance in distributed Bragg reflectors-based ultrathin highly absorbing dielectric and its application in solar cells

Xu-Lin Zhang,[1] Jun-Feng Song,[1,2,a)] Xian-Bin Li,[1] Jing Feng,[1] and Hong-Bo Sun[1,a)]
[1]*State Key Laboratory on Integrated Optoelectronics, College of Electronic Science and Engineering, Jilin University, 2699 Qianjin Street, Changchun 130012, China*
[2]*Institute of Microelectronics, A*STAR (Agency for Science, Technology and Research), 11 Science Park Road, Singapore Science Park II, Singapore 117685*

(Received 15 January 2013; accepted 27 February 2013; published online 12 March 2013)

We present a design of anti-reflection resonance in distributed Bragg reflectors (DBRs) based ultrathin highly absorbing dielectric. In such structure, anti-reflection resonance can be supported at wavelengths much longer than those achieved by the previous metal-based structure due to the appropriate reflection phase from the DBRs surface. The proposed anti-reflection resonance can find applications in thin-film organic solar cells for light trappings. By replacing partial metal electrode with DBRs to provide the desired reflection phase, the overall absorptivity can be greatly increased by ~31% due to the good matching between anti-reflection resonance and high-absorption range of the active layers. © *2013 American Institute of Physics*. [http://dx.doi.org/10.1063/1.4795286]

Resonant optical cavity configurations, such as the asymmetrical Fabry-Perot (FP) cavity using a dielectric as the cavity, have been studied extensively for applications of modulators,[1,2] detectors,[3,4] perfect absorbers,[5] and solar cells.[6] Enhanced absorption can be achieved in these devices associated with enhanced performance by the critical coupling, which facilitates more power into the cavity through a well-known effect called as anti-reflection resonance.[1–6] On anti-reflection resonance, minimized reflection can be realized as a result of the destructive interference of the partial reflection waves. Apart from the asymmetrical FP cavity, other anti-reflection structures with various fabrication methods have also been studied, such as the non-reflecting silicon and polymer surfaces fabricated by plasma etching and replication,[7] broadband anti-reflection by integrating antireflective nanoislands with silicon nanoconical-frustum arrays,[8] and pseudoperiodic antireflective subwavelength structures by using self-assembled etch masks.[9] Although the fabrications of these structures are fast and cost-effective, the asymmetrical FP cavity is still a simpler anti-reflection structure and therefore draws much attentions. However, the formation of anti-reflection resonance in the asymmetrical FP cavity requires the thickness of the dielectric cavity to be at least of a quarter-wavelength ($\lambda/4n$, where n is the refractive index of the dielectric), which limits it from ultrathin-film-related applications, such as those in small molecules based organic solar cells (OSCs), whose active layers are required to be typically thinner than 30 nm in view of the short diffusion length of the exitons.[10–12]

Recently, a concept has been proposed that the anti-reflection resonance can be supported in a metal based asymmetrical FP cavity comprising ultrathin (~5–20 nm) highly absorbing dielectric, which is much thinner than the quarter-wavelength ($\lambda \sim 600$ nm).[13] The breakthrough of the quarter-wavelength limitation benefits from the significant extinction coefficient of the dielectric, which can provide nontrivial phase shifts at interfaces and create the anti-reflection resonance. This concept has been then applied in an ultrathin ($\sim\lambda/65$) perfect absorber.[14] Inspired by these progresses, applications in ultrathin solar cells can be expected and are needed to be investigated.

In this work, we investigate the anti-reflection resonance in ultrathin highly absorbing dielectric for applications of OSCs. We find that with an ultrathin (~15 nm) dielectric, the resonant wavelength in the metal based asymmetrical FP cavity could not match well with the high-absorption wavelength range of OSCs. We show that such obstacle can be overcome by replacing the metal with distributed Bragg reflectors (DBRs). In the DBRs based structure, anti-reflection resonance can be supported at wavelengths much longer than those achieved by the metal-based structure due to the appropriate reflection phase from the DBRs surface. Then we apply the anti-reflection resonance to, for a proof-of-concept demonstration, small molecules based OSCs to improve the absorption performance. We find that by replacing partial metal electrode with DBRs, the overall absorptivity can be greatly increased by ~31% due to the good matching between anti-reflection resonance and high-absorption range of the active layers.

Schematics of the studied asymmetrical FP cavities are shown in Fig. 1(a). We consider transverse-electric (TE) polarized normal incidence from air (medium 1) onto a highly absorbing dielectric (medium 2) with complex refractive index (RI) $n_2 = 2 + 1i$ and thickness d_2, which is deposited on reflecting substrates (medium 3). Opaque metal (~Ag) is used as the reflecting substrate for structure A. Similar structures have been recently studied in the work of Kats *et al.*[13,14] We first apply the transfer matrix method[15] to calculate the absorptivity spectra in the absorbing dielectric for structure A. The results are shown in Fig. 1(b), where absorption peaks can be seen at wavelengths of ~360 nm, 455 nm, and 586 nm for cases of $d_2 = 15$ nm, 35 nm, and 55 nm, respectively. These absorption peaks with the dielectric much thinner than

a)Authors to whom correspondence should be addressed. Electronic addresses: songjf@ime.a-star.edu.sg and hbsun@jlu.edu.cn.

the quarter-wavelength are a result of the significant extinction coefficient of the dielectric ($\sim 1i$), which can provide non-trivial phase shifts at interfaces and create an anti-reflection resonance.[13,14] More specifically, the reflection coefficient r in such asymmetrical FP cavity for TE-polarized normal incidence can be written as[16]

$$r = \sum_{m=0}^{\infty} r_m = \frac{r_{12} + r_{23}\exp(2i\beta)}{1 + r_{12}r_{23}\exp(2i\beta)}, \quad (1)$$

where r_m is the m roundtrip reflection coefficient by $r_m = t_{12} r_{23}^{m} r_{21}^{m-1} t_{21} \exp(2mi\beta)$, r_{pq} and t_{pq} are the Fresnel reflection and transmission coefficients from medium p to medium q given by $r_{pq} = (n_p - n_q)/(n_p + n_q)$ and $t_{pq} = 2n_p/(n_p + n_q)$, and $\beta = 2\pi n_2 d_2/\lambda$. On anti-reflection resonance, the numerator of r, defined as r_n, exhibits a minimum associated with enhanced absorption in the dielectric.

The anti-reflection resonance in the ultrathin highly absorbing dielectric may be valuable for applications in solar cells. In this study, we focus on small molecules based OSCs. The absorption performance of the OSCs can be improved if the anti-reflection resonance is designed to overlap well with the high-absorption wavelength range of the active layers. Most active media applied in OSCs (e.g., CuPc, SubPc) exhibit a complex RI in the high-absorption wavelength range comparable to that of the medium 2 in Fig. 1(a). However, such high-absorption wavelength range always locates at 550 nm–650 nm, which is much longer than the absorption peak of ~360 nm for the case of $d_2 = 15$ nm in Fig. 1(b). Although the absorption peak can be tuned by increasing d_2, drawbacks are twofold. First, the active layers are required to be very thin (typically, less than 30 nm) in view of the short diffusion length of exitons in small molecules based OSCs.[10–12] Second, light absorption in a thicker dielectric may be already sufficient, which means the anti-reflection resonance would not contribute to the absorption enhancement as significantly as that in a thinner dielectric. Therefore, advanced designs are required to create an anti-reflection resonance at these desired longer wavelengths with the dielectric still being thinner.

To achieve such anti-reflection resonance, we need to redesign the structure by considering the numerator of r,

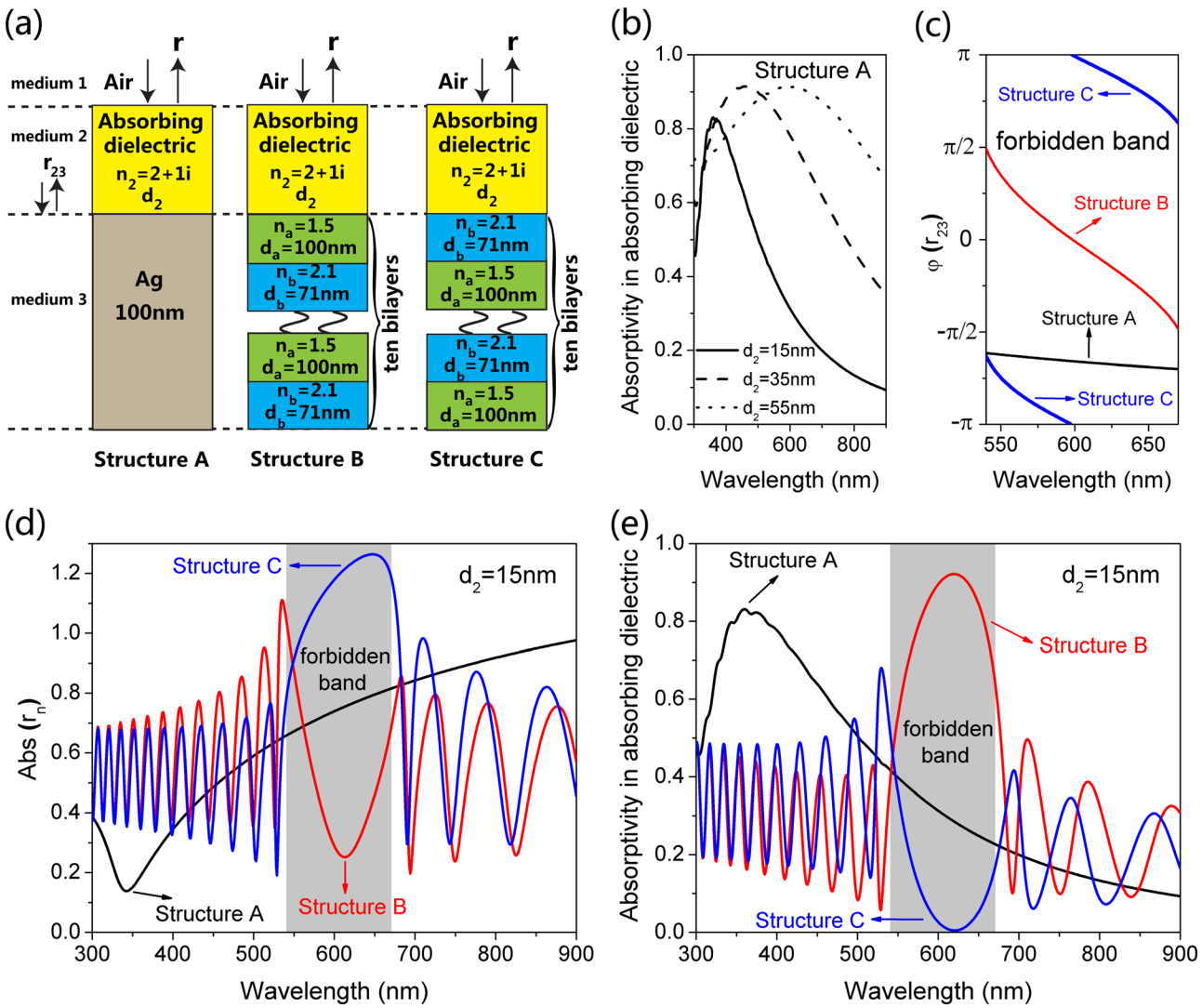

FIG. 1. (a) Schematics of the asymmetrical FP cavity comprising ultrathin highly absorbing dielectric with $n_2 = 2 + 1i$. The reflecting substrates are chosen as Ag, DBRs starting with a layer of low RI, and DBRs starting with a layer of high RI for structures A, B, and C, respectively. (b) Absorptivity spectra in the absorbing dielectric for structure A with different dielectric thicknesses. (c) Phases of the term r_{23} for the three structures in the Bragg forbidden band. (d) Amplitudes of the term r_n and (e) absorptivity spectra in the absorbing dielectric for the three structures with the dielectric thickness of 15 nm.

which is $r_n = r_{12} + r_{23}\exp(2i\beta)$. Once n_2 and d_2 are chosen, r_{12} and $\exp(2i\beta)$ are fixed, whereas the only tunable term is r_{23}, which strongly depends on the characteristics of the reflecting substrate. Our approach is to tune the phase of $r_{23}(\varphi(r_{23}))$, as its amplitude may be always close to unity. The tuning can be realized by using, instead of the metal, DBRs as the reflecting substrate. The designed structures are shown in Fig. 1(a) as structure B and structure C, respectively, where the only difference between the two structures is the sequence of the DBR bilayers. The DBR parameters are chosen as $n_a = 1.5$, $n_b = 2.1$, $d_a = 100$ nm, and $d_b = 71$ nm. For normal incidence, the Bragg forbidden band can be calculated[17] as 540 nm–670 nm, with the Bragg wavelength located at ~600 nm. Then we calculate $\varphi(r_{23})$ for the three structures, with the results shown in Fig. 1(c) for the Bragg forbidden band. We find that $\varphi(r_{23})$ is almost invariable for structure A, whereas phases from nearly $-\pi$ to $+\pi$ can be achieved by structure B and structure C. Such large scale variation of $\varphi(r_{23})$ may provide various possibilities of r_n, and anti-reflection resonance in the proposed DBR based structures is expected.

We calculate the absolute value of r_n (Abs(r_n)) for the three structures to verify our previous supposition. The results are shown in Fig. 1(d) for $d_2 = 15$ nm, where the grey region corresponds to the forbidden band. As expected, a minimum of Abs(r_n) turns up at ~610 nm for structure B, whereas a maximum shows up inside the forbidden band for structure C. These minimum and maximum are associated with an absorption peak and dip, respectively, as shown by the absorptivity spectra of the absorbing dielectric in Fig. 1(e). To further verify the mechanism of the anti-reflection resonance, we give the phasor diagram of reflected partial waves at the wavelength of 610 nm for the three structures in Fig. 2. It is noted that the partial wave r_0 is the same for the three structures, while the amplitude of r_m ($m > 0$) decreases as m increases due to the highly absorbing property of the dielectric. So the partial wave $r_1 = t_{12}r_{23}t_{21}\exp(2i\beta)$ is crucial for the reflection properties. This term only depends on $\varphi(r_{23})$ as shown in Fig. 1(c), which directly cause the different trajectory of r_1 in Fig. 2, making the phasor return back near the origin for structure B but move far away from the origin for structure C. Therefore, an anti-reflection resonance has been realized in the proposed DBRs based structure B due to the appropriate reflection phase of the DBRs. The superiority of such structure is that the anti-reflection resonance can be tuned freely only by designing the Bragg forbidden band and a resonant wavelength longer than the one in the metal based structure A can be achieved. Although similar structures have been proposed before,[5] they applied the quarter-wavelength resonance where a spacer layer (~90 nm) was needed. Our design follows the work of Kats *et al.*[13,14] by applying the large extinction coefficient, where the dielectric (~15 nm) can be far thinner than the quarter-wavelength (~75 nm).

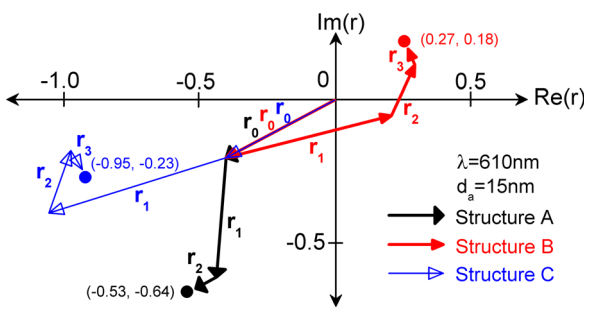

FIG. 2. Phasor diagrams of reflected partial waves at the wavelength of 610 nm for the three structures with the dielectric thickness of 15 nm, where the phasor returns back near the origin associated with anti-reflection resonance in structure B.

Then we discuss the potential application of the anti-reflection resonance in OSCs. A schematic of the studied OSC is shown as device A in Fig. 3(a). This CuPc-PTCBI based thin-film OSC has been used as a model to investigate the surface plasmon polaritons (SPPs) based scheme for light trappings in some previous literatures.[10,11] Here, we choose the same structure parameters to study the anti-reflection resonance based scheme. As the total organic layers are too thin (~47 nm) to support an anti-reflection resonance in the high-absorption range (600 nm–700 nm, see Fig. 3(b)) of the active layers for device A, designs as device B and device C are proposed by replacing partial metal electrode with DBRs. Although 15 nm-thick Ag is still remained as the electrode, the reflection phase on the metal surface, termed as $\varphi(r_{23})$, can be greatly expanded for device B and device C as shown in Fig. 3(c). Therefore, anti-reflection resonance can be expected. The RIs, thicknesses, and number of the DBR bilayers are given by n_A, n_B, d_A, d_B, and N_{DBR}, respectively. The RIs of the organic layers are extracted from our previous experimental data.[12,18]

The DBRs are first considered as six alternating bilayers of CaF_2 and TiO_2, with the RIs simply as $n_A = 1.3$ and $n_B = 2.7$. We apply the overall absorptivity A_{Total} as criteria for the absorption performance of the OSCs.[10,19] It can be calculated by $A_{Total} = \frac{\int_{400nm}^{900nm} a(\lambda)S(\lambda)d\lambda}{\int_{400nm}^{900nm} S(\lambda)d\lambda}$, where $a(\lambda)$ is the absorption spectra in the active layers for normal TE- or TM-polarized incidence, and $S(\lambda)$ is the solar irradiance spectrum under AM1.5 illumination. We calculate the overall absorptivity for device B and device C by choosing different combinations of d_A and d_B. The results are shown in Figs. 3(d) and 3(e), where the blue star corresponds to the best choice of $d_A = 145$ nm and $d_B = 53$ nm for device B. At this point, the absorptivity spectra in the active layers under normal TE-polarized incidence for device A, device B, and device C are shown in Fig. 3(b) by the black line, red-circle line, and blue-square line, respectively. We find that device B exhibits considerable absorption enhancement with an overall absorptivity of ~0.204, which is 31% higher than that for device A (~0.156) due to the appropriate reflection phase induced anti-reflection resonance. In contrast, the absorption performance for device C is even worse than that for device A as a result of the inappropriate reflection phase induced enhanced reflection. Therefore, the anti-reflection resonance can only be achieved in such OSC with the DBRs starting with a layer of a low RI.

The absorption performance of the three devices can also be revealed from the profiles of the electric field intensity enhancement $|E|/|E_0|$ (E_0 corresponds to the incidence) as shown in Figs. 4(a)–4(c). An enlarged view of the dashed

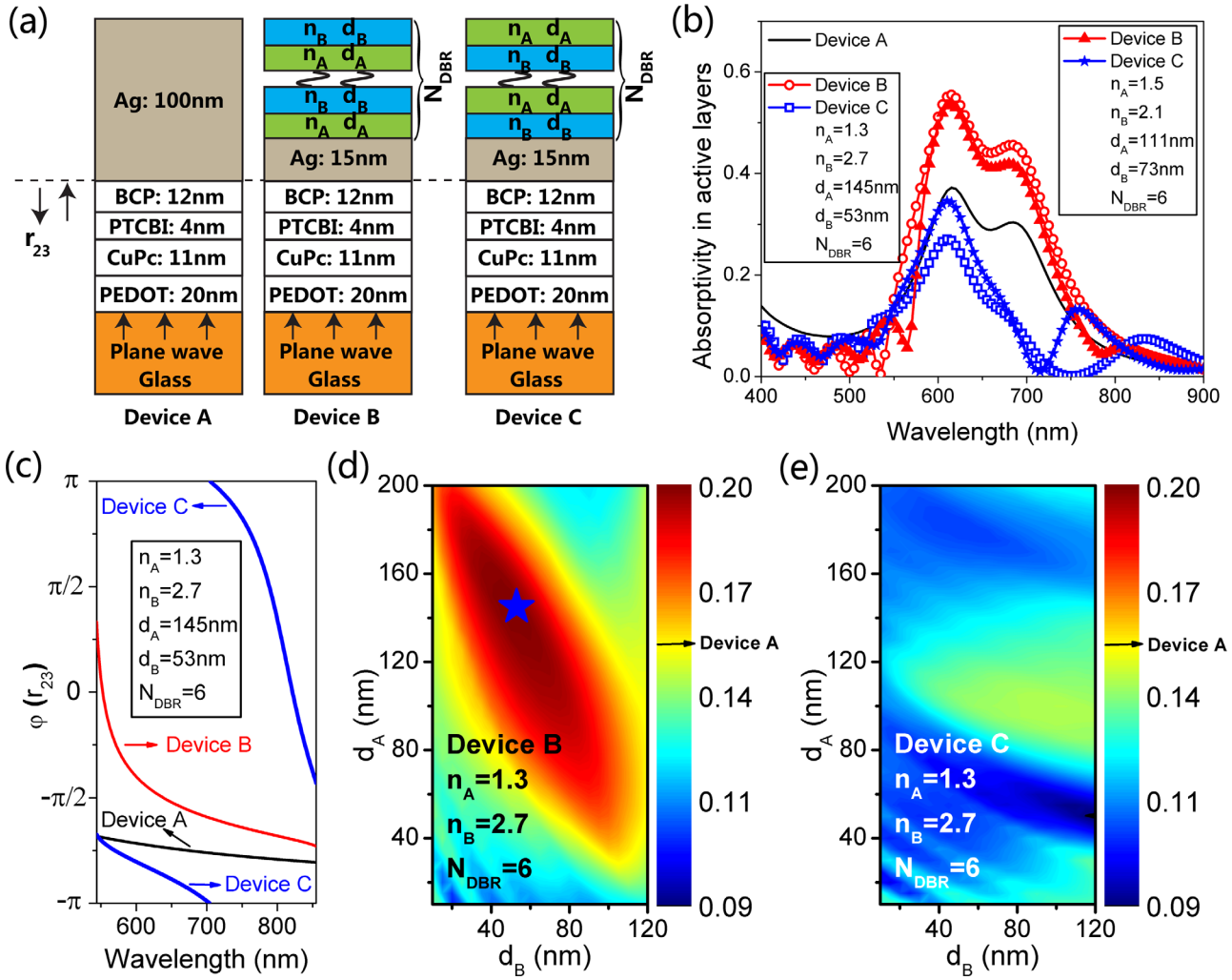

FIG. 3. (a) Schematics of the CuPc-PTCBI based OSCs. Device A corresponds to a reference OSC, while device B and device C are the proposed DBR based OSCs, where partial metal electrodes are replaced with DBRs. (b) Absorptivity spectra in the active layers for device A (black line), device B (red-symbol lines), and device C (blue-symbol lines) with the DBR parameters indicated in the figure. (c) Phases of the term r_{23} for the three devices in the Bragg forbidden band. (d) and (e) Overall absorptivity for (d) device B and (e) device C with different combinations of DBR thicknesses, where the RIs are indicated in the figures.

rectangular region is represented below each figure. We find that compared with device A, device B exhibits a stronger field enhancement in the active layers for the high-absorption range (600 nm–700 nm), which brings the absorption enhancement in Fig. 3(b). However, a field decrement can be seen in the active layers for device C, which results in enhanced reflection associated with decreased absorption.

Then we investigate the absorption performance of the OSCs with the DBRs exhibiting a lower RIs contrast as $n_A = 1.5$ and $n_B = 2.1$. The thicknesses of the bilayers are optimally chosen as $d_A = 111$ nm and $d_B = 73$ nm. The absorptivity spectra for device B and device C with such DBR parameters are shown in Fig. 3(b) by the red-triangle line and blue-star line, respectively, in order to compare with the aforementioned devices ($n_A = 1.3$, $n_B = 2.7$, $d_A = 145$ nm, $d_B = 53$ nm). We find that the device B with a lower RIs contrast exhibits a narrower band absorption enhancement associated with smaller overall absorptivity (~0.182) than that for the device B with a higher RIs contrast (~0.204). Such difference may be involved with the fact that DBRs with a lower RIs contrast exhibit a narrower Bragg forbidden band.[17] Therefore, DBRs with a higher RIs contrast are preferred in the proposed anti-reflection resonance based OSCs.

Finally, we consider the effect of the number of DBR bilayers on the overall absorptivity. The results are shown in Fig. 5 for device A, device B, and device C by the black dashed line, red-symbol lines, and blue-symbol lines, respectively. The thicknesses of the DBR bilayers are optimally chosen in consideration of the best absorption performance for device B in each case. We find that about four to six bilayers are already sufficient for device B to achieve considerable absorption enhancement, whereas the overall absorptivity for device C is always lower than that for device A. Although a similar design[20] was proposed recently by replacing partial metal with DBRs, the DBRs were used simply as reflectors for the semitransparent solar cell, whereas the DBRs are used for providing the reflection phase in our work. Our design also shows values for semitransparent OSCs.

In summary, we have proposed a design of anti-reflection resonance in DBRs based ultra-thin highly absorbing dielectric and discussed the application in thin-film OSCs. To achieve a better absorption performance, partial metal electrode should be replaced with DBRs exhibiting a higher RIs contrast. The overall absorptivity can be greatly increased by ~31% due to the anti-reflection resonance. The same OSCs have been studied previously by replacing partial

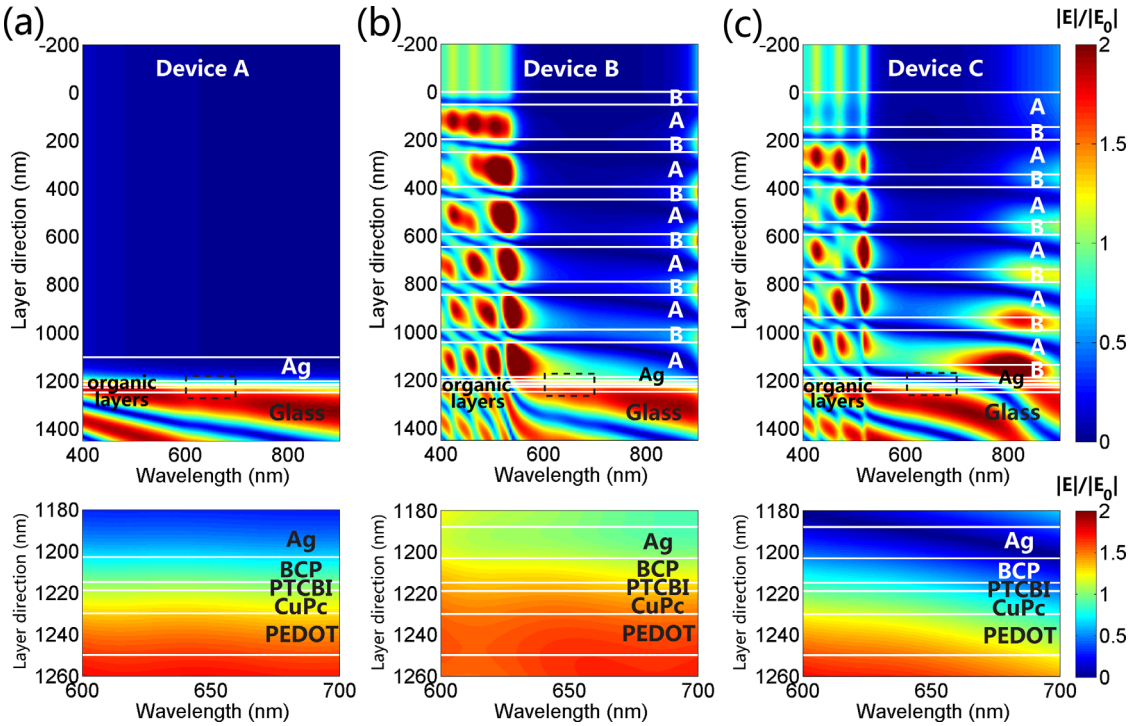

FIG. 4. (a)–(c) Profiles of the electric field intensity enhancement for (a) device A, (b) device B, and (c) device C, where the DBR parameters are chosen as $n_A = 1.3$, $n_B = 2.7$, $d_A = 145$ nm, and $d_B = 53$ nm. An enlarged view of the dashed rectangular region is represented below each figure.

poly(3,4-ethylenedioxythiophene) (PEDOT) layer with metal to realize a metallic grating[10] or introducing double metallic gratings,[11] where the overall absorptivity can be increased by ~50% or ~67%, respectively. In such devices, the improvement of the absorption performance is a result of the large field enhancement in the active layers, which is induced by the excitations of SPPs modes. Although the achieved absorption enhancement in our device is lower than that in the aforementioned SPPs scheme based OSCs, it only requires simple fabrications of planar structures, in contrast to the requirement for complicated nanofabrications of metallic gratings[10–12,18,21] or nanoparticles[22] in the SPPs based devices. Moreover, the discussed schemes may not be conflicting in some cases. For instance, by introducing metallic gratings in our device, the absorption performance may be further improved through the coupling of anti-reflection resonance and SPPs.

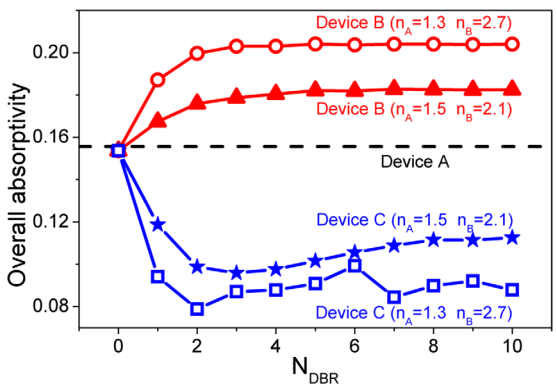

FIG. 5. Overall absorptivity as a function of the number of DBR bilayers for device A (black dashed line), device B (red-symbol lines), and device C (blue-symbol lines) with the DBR parameters indicated in the figure.

The authors acknowledge the support from NSFC (Grant Nos. 90923037, 61137001, 61107024, and 61177090).

[1]R. H. Yan, R. J. Simes, and L. A. Coldren, IEEE Photon. Technol. Lett. **1**, 273 (1989).
[2]K. K. Law, R. H. Yan, L. A. Coldren, and J. L. Merz, Appl. Phys. Lett. **57**, 1345 (1990).
[3]A. Chin and T. Y. Chang, J. Vac. Sci. Technol. B **8**, 339 (1990).
[4]K. Kishino, M. S. Unlu, J. I. Chyi, J. Reed, L. Arsenault, and H. Morkoc, IEEE J. Quantum Electron. **27**, 2025 (1991).
[5]J. R. Tischler, M. S. Bradley, and V. Bulovic, Opt. Lett. **31**, 2045 (2006).
[6]Y. B. Long, Appl. Phys. Lett. **99**, 093310 (2011).
[7]L. Sainiemi, V. Jokinen, A. Shah, M. Shpak, S. Aura, P. Suvanto, and S. Franssila, Adv. Mater. **23**, 122 (2011).
[8]H. Park, D. Shin, G. Kang, S. Baek, K. Kim, and W. J. Padilla, Adv. Mater. **23**, 5796 (2011).
[9]Y. Ou, V. Jokubavicius, R. Yakimova, M. Syväjärvi, and H. Ou, Opt. Lett. **37**, 3816 (2012).
[10]C. Min, J. Li, G. Veronis, J. Y. Lee, S. Fan, and P. Peumans, Appl. Phys. Lett. **96**, 133302 (2010).
[11]M. A. Sefunc, A. K. Okyay, and H. V. Demir, Appl. Phys. Lett. **98**, 093117 (2011).
[12]Y. Jin, J. Feng, X. L. Zhang, M. Xu, Y. G. Bi, Q. D. Chen, H. Y. Wang, and H. B. Sun, Appl. Phys. Lett. **101**, 163303 (2012).
[13]M. A. Kats, R. Blanchard, P. Genevet, and F. Capasso, Nature Mater. **12**, 20 (2013).
[14]M. A. Kats, D. Sharma, J. Lin, P. Genevet, R. Blanchard, Z. Yang, M. M. Qazilbash, D. N. Basov, S. Ramanathan, and F. Capasso, Appl. Phys. Lett. **101**, 221101 (2012).
[15]P. Yeh, *Optical Waves in Layered Media* (Wiley, New York, 1988).
[16]M. Born and E. Wolf, *Principles of Optics*, 7th ed. (Cambridge University Press, Cambridge, 2003).
[17]P. Yeh, A. Yariv, and C. S. Hong, J. Opt. Soc. Am. **67**, 423 (1977).
[18]Y. Jin, J. Feng, X. L. Zhang, Y. G. Bi, Y. Bai, L. Chen, T. Lan, Y. F. Liu, Q. D. Chen, and H. B. Sun, Adv. Mater. **24**, 1187 (2012).
[19]X. L. Zhang, J. F. Song, X. B. Li, J. Feng, and H. B. Sun, Appl. Phys. Lett. **101**, 243901 (2012).
[20]W. J. Yu, L. Shen, Y. B. Long, W. B. Guo, F. X. Meng, S. P. Ruan, X. Jia, H. S. Ma, and W. Y. Chen, Appl. Phys. Lett. **101**, 153307 (2012).
[21]X. L. Zhang, J. Feng, J. F. Song, X. B. Li, and H. B. Sun, Opt. Lett. **36**, 3915 (2011).
[22]Y. H. Su, Y. F. Ke, S. L. Cai, and Q. Y. Yao, Light: Sci. Appl. **1**, e14 (2012).